



The First Post-Kepler Brightness Dips of KIC 8462852

Tabetha. S. Boyajian¹ , Roi Alonso^{2,3}, Alex Ammerman⁴, David Armstrong^{5,6}, A. Asensio Ramos^{2,3}, K. Barkaoui^{7,8}, Thomas G. Beatty^{9,10}, Z. Benkhaldoun⁸, Paul Benni^{11,12}, Rory O. Bentley¹, Andrei Berdyugin¹³, Svetlana Berdyugina¹⁴, Serge Bergeron^{11,15}, Allyson Bieryla¹⁶, Michaela G. Blain¹⁷, Alicia Capetillo Blanco¹¹, Eva H. L. Bodman^{18,123}, Anne Boucher¹⁹, Mark Bradley¹¹, Stephen M. Brincat¹¹, Thomas G. Brink²⁰, John Briol¹¹, David J. A. Brown^{5,6}, J. Budaj²¹, A. Burdanov⁷, B. Cale²², Miguel Aznar Carbo²³, R. Castillo García^{11,24,25}, Wendy J. Clark¹¹, Geoffrey C. Clayton¹ , James L. Clem²⁶, Phillip H Coker¹¹, Evan M. Cook¹⁷, Chris M. Copperwheat²⁷, J. L. Curtis²⁸, R. M. Cutri²⁹, B. Cseh³⁰, C. H. Cynamon^{11,31}, Alex J. Daniels²⁶, James R. A. Davenport^{32,124} , Hans J. Deeg^{2,3}, Roberto De Lorenzo³³, Thomas de Jaeger²⁰, Jean-Bruno Desrosiers¹¹, John Dolan^{5,6}, D. J. Dowhos^{11,34}, Franky Dubois³⁵, R. Durkee³⁶, Shawn Dvorak¹¹, Lynn Easley¹¹, N. Edwards³⁷, Tyler G. Ellis¹, Emery Erdelyi¹¹, Steve Ertel³⁸, Rafael. G. Farfán³⁹, J. Farihi⁴⁰ , Alexei V. Filippenko^{20,125}, Emma Foxell^{5,6}, Davide Gandolfi⁴¹, Faustino Garcia^{42,43}, F. Giddens⁴⁴, M. Gillon⁷, Juan-Luis González-Carballo^{11,45}, C. González-Fernández⁴⁶, J. I. González Hernández^{2,3}, Keith A. Graham¹¹, Kenton A. Greene¹⁷, J. Gregorio⁴⁷, Na'ama Hallakoun⁴⁸ , Ottó Hanyecz^{30,49} , G. R. Harp⁵⁰, Gregory W. Henry⁵¹, E. Herrero⁵², Caleb F. Hildbold²⁶, D. Hinzel¹¹, G. Holgado^{2,3}, Bernadett Ignácz^{30,49}, Ilya Ilyin⁵³, Valentin D. Ivanov^{54,55}, E. Jehin⁷, Helen E. Jermak²⁷, Steve Johnston¹¹, S. Kafka¹¹, Csilla Kalup^{30,49}, Emmanuel Kardasis⁵⁶, Shai Kaspi⁴⁸, Grant M. Kennedy⁵ , F. Kiefer⁵⁷, C. L. Kieley⁵⁸, Dennis Kessler⁵⁹, H. Kiiskinen⁶⁰, T. L. Killestein^{11,61}, Ronald A. King¹¹, V. Kollar²¹, H. Korhonen⁶² , C. Kotnik¹¹, Réka Könyves-Tóth^{30,49}, Levente Kriskovics³⁰ , Nathan Krumm¹¹, Vadim Krushinsky⁶³, E. Kundra²¹, Francois-Rene Lachapelle¹⁹, D. LaCourse⁶⁴, P. Lake^{11,65,66}, Kristine Lam^{5,6}, Gavin P. Lamb²⁷ , Dave Lane⁶⁷, Marie Wingyee Lau⁶⁸ , Pablo Lewin^{11,69}, Chris Lintott⁷⁰ , Carey Lisse⁷¹ , Ludwig Logie³⁵, Nicolas Longeard⁷², M. Lopez Villanueva⁷³, E. Whit Ludington^{11,74}, A. Mainzer⁷⁵, Lison Malo^{76,77}, Chris Maloney¹¹, A. Mann⁷⁸, A. Mantero¹¹, Massimo Marengo⁷⁹ , Jon Marchant²⁷, M. J. Martínez González^{2,3}, Joseph R. Masiero⁸⁰ , Jon C. Mauerhan²⁰, James McCormac^{5,6}, Aaron McNeely^{4,11}, Huan Y. A. Meng³⁸ , Mike Miller^{11,81}, Lawrence A. Molnar¹⁷ , J. C. Morales⁸², Brett M. Morris⁸³ , Matthew W. Muterspaugh^{51,84}, David Nespral^{2,3}, C. R. Nugent⁸⁵, Katherine M. Nugent¹, A. Odasso^{11,34}, Derek O'Keeffe^{11,86}, A. Oksanen⁶⁰, John M. O'Meara⁸⁷ , András Ordasi³⁰, Hugh Osborn^{5,6,88}, John J. Ott¹¹, J. R. Parks⁸⁹, Diego Rodriguez Perez¹¹, Vance Petriew^{11,15}, R. Pickard⁹⁰, András Pál³⁰ , P. Plavchan²², Don Pollacco^{5,6}, F. Pozo Nuñez^{91,92} , F. J. Pozuelos⁷, Steve Rau³⁵, Seth Redfield⁹³ , Howard Relles¹⁶, Ignasi Ribas⁸², Jon Richards^{94,95}, Joonas L. O. Saario^{96,97} , Emily J. Safron¹ , J. Martin Sallai^{30,49}, Krisztián Sárneczky³⁰ , Bradley E. Schaefer¹, Clea F. Schumer¹⁶, Madison Schwartzendruber⁴, Michael H. Siegel⁹⁸, Andrew P. V. Siemion^{99,100,101}, Brooke D. Simmons^{102,126} , Joshua D. Simon¹⁰³, S. Simón-Díaz^{2,3}, Michael L. Sitko^{104,105}, Hector Socas-Navarro^{2,3}, Á. Sódor³⁰, Donn Starkey¹⁰⁶, Iain A. Steele²⁷, Geoff Stone^{11,107} , Klaus G. Strassmeier⁵³, R. A. Street¹⁰⁸, Tricia Sullivan²⁷, J. Suomela¹⁰⁹, J. J. Swift³⁷, Gyula M. Szabó¹¹⁰, Róbert Szabó³⁰ , Róbert Szakáts³⁰ , Tamás Szalai¹¹¹, Angelle M. Tanner¹¹², B. Toledo-Padrón^{2,3}, Tamás Tordai¹¹³, Amaury H. M. J. Triaud¹¹⁴, Jake D. Turner¹¹⁵, Joseph H. Ulowetz¹¹, Marian Urbanik^{11,116}, Siegfried Vanaverbeke^{35,117}, Andrew Vanderburg¹¹⁸, Krisztián Vida³⁰ , Brad P. Vietje¹¹, József Vinkó³⁰ , K. von Braun¹¹⁹, Elizabeth O. Waagen¹¹, Dan Walsh⁴, Christopher A. Watson¹²⁰, R. C. Weir¹¹, Klaus Wenzel¹²¹, C. Westendorp Plaza^{2,3}, Michael W. Williamson⁵¹, Jason T. Wright^{9,10,127} , M. C. Wyatt¹²², WeiKang Zheng²⁰, and Gabriella Zsidi^{30,49}

¹ Department of Physics and Astronomy, Louisiana State University, Baton Rouge, LA 70803 USA; boyajian@lsu.edu

² Instituto de Astrofísica de Canarias, E-38205 La Laguna, Tenerife, Spain

³ Departamento de Astrofísica, Universidad de La Laguna, E-38206 La Laguna, Tenerife, Spain

⁴ University of Notre Dame QuarkNet Center, Notre Dame, IN, USA

⁵ Department of Physics, University of Warwick, Gibbet Hill Road, Coventry, CV4 7AL, UK

⁶ Centre for Exoplanets and Habitability, University of Warwick, Gibbet Hill Road, Coventry, CV4 7AL, UK

⁷ Space sciences, Technologies and Astrophysics Research (STAR) Institute, Université de Liège, Belgium

⁸ Laboratoire LPHEA, Oukaimeden Observatory, Cadi Ayyad University/FSSM, BP 2390, Marrakesh, Morocco

⁹ Department of Astronomy & Astrophysics, The Pennsylvania State University, 525 Davey Lab, University Park, PA 16802, USA

¹⁰ Center for Exoplanets and Habitable Worlds, The Pennsylvania State University, 525 Davey Lab, University Park, PA 16802, USA

¹¹ American Association of Variable Star Observers (AAVSO)

¹² Acton Sky Portal, Acton, MA 01720, USA

¹³ Tuorla Observatory, University of Turku, Finland

¹⁴ Kiepenheuer Institut für Sonnenphysik, Freiburg, Germany

¹⁵ The Royal Astronomical Society of Canada, Canada

¹⁶ Harvard-Smithsonian Center for Astrophysics, 60 Garden Street, Cambridge, MA 02138, USA

¹⁷ Department of Physics and Astronomy, Calvin College, Grand Rapids, MI 49546, USA

¹⁸ School of Earth and Space Exploration, Arizona State University, Tempe, AZ 85287-1404, USA

¹⁹ Institute for Research on Exoplanets, Département de physique, Université de Montréal, Montréal, QC H3C 3J7, Canada

²⁰ Department of Astronomy, University of California, Berkeley, CA 94720-3411, USA

²¹ Astronomical Institute, Slovak Academy of Sciences, The Slovak Republic

²² George Mason University, 4400 University Drive, MSN 3F3, Fairfax, VA 22030, USA

²³ American Association of Variable Star Observers, Blesa, Spain

²⁴ Asociación Astronómica Cruz del Norte, Alcobendas, Madrid, Spain

²⁵ MPC Z83 Chicharronian Tres Cantos Observatory, Tres Cantos, Madrid, Spain

²⁶ Department of Physics, Grove City College, 100 Campus Drive, Grove City, PA 16127, USA

²⁷ Astrophysics Research Institute, Liverpool John Moores University, 146 Brownlow Hill, L3 5RF, UK

- ²⁸ Department of Astronomy, Columbia University, 550 West 120th Street, New York, NY 10027, USA
- ²⁹ IPAC, Mail Code 100-22, California Institute of Technology, 1200 E. California Boulevard, Pasadena, CA 91125, USA
- ³⁰ MTA CSFK, Konkoly Observatory, Budapest, Hungary
- ³¹ Howard Astronomical League, Columbia, MD, USA
- ³² Department of Physics and Astronomy, Western Washington University, 516 High Street, Bellingham, WA 98225, USA
- ³³ Alghard Observatory, Ostuni, MPC Code K82, Italy
- ³⁴ Sierra Stars Observatory Network, Canada
- ³⁵ Astrolab IRIS, Verbrandemolenstraat, Ypres, Belgium and Vereniging voor Sterrenkunde, Werkgroep Veranderlijke Sterren, Belgium
- ³⁶ Shed of Science Observatory, 5213 Washburn Avenue S., Minneapolis, MN 55410, USA
- ³⁷ The Thacher School, 5025 Thacher Road, Ojai, CA 93023, USA
- ³⁸ Steward Observatory, Department of Astronomy, University of Arizona, 933 North Cherry Avenue, Tucson, AZ 85721, USA
- ³⁹ Observatorio Astronómico URANIBORG; E-41400 Écija, Sevilla, Spain
- ⁴⁰ Physics and Astronomy, University College London, London WC1E 6BT, UK
- ⁴¹ Dipartimento di Fisica, Università di Torino, via P. Giuria 1, I-10125 Torino, Italy
- ⁴² M1 Group, Spain
- ⁴³ La Vara, Valdés Observatory-MPC J38, Spain
- ⁴⁴ Missouri State University, 901 S National Avenue, Springfield, MO 65897, USA
- ⁴⁵ MPC I84 Observatorio Cerro del Viento, Badajoz, Spain
- ⁴⁶ Institute of Astronomy, University of Cambridge, Madingley Road, CB3 0HA, UK
- ⁴⁷ Atalaia Group and CROW Observatory Portalegre, Portugal
- ⁴⁸ School of Physics and Astronomy and Wise Observatory, Raymond and Beverly Sackler Faculty of Exact Sciences, Tel Aviv University, Tel Aviv 69978, Israel
- ⁴⁹ Loránd Eötvös University, Budapest, Hungary
- ⁵⁰ SETI Institute, 189 Bernardo, Suite 200, Mountain View, CA 94043, USA
- ⁵¹ Center of Excellence in Information Systems, Tennessee State University, Nashville, TN 37209, USA
- ⁵² Montsec Astronomical Observatory (OAdM), Institut d'Estudis Espacials de Catalunya (IEEC), Barcelona, Spain
- ⁵³ Leibniz-Institute for Astrophysics Potsdam (AIP), An der Sternwarte 16, D-14482 Potsdam, Germany
- ⁵⁴ European Southern Observatory, Ave. Alonso de Córdova 3107, Vitacura, Santiago, Chile
- ⁵⁵ European Southern Observatory, Karl-Schwarzschild-Str. 2, D-85748, Garching bei München, Germany
- ⁵⁶ Hellenic Amateur Astronomy Association, Greece
- ⁵⁷ Institut d'Astrophysique de Paris, UMR7095 CNRS, Université Pierre & Marie Curie, 98 bis boulevard Arago, F-75014 Paris, France
- ⁵⁸ Department of Physics and Astronomy, University of Victoria, Victoria, BC, V8W 3P2, Canada
- ⁵⁹ Ott Observatory, Nederland, CO 80466, USA
- ⁶⁰ Hankasalmi Observatory, Hankasalmi, Finland
- ⁶¹ British Astronomical Association, Variable Star Section, UK
- ⁶² Dark Cosmology Centre, University of Copenhagen, Juliane Maries Vej 30, DK-2100 Copenhagen Ø, Denmark
- ⁶³ Kouroukva observatory, Ural Federal University, Russia
- ⁶⁴ Amateur Astronomer, USA
- ⁶⁵ Astronomy Society Victoria, Australia
- ⁶⁶ iTelescope.net, Siding Spring, Australia
- ⁶⁷ Saint Mary's University, The Royal Astronomical Society of Canada, Canada
- ⁶⁸ Department of Astronomy and Astrophysics, UCO/Lick Observatory, University of California, 1156 High Street, Santa Cruz, CA 95064, USA
- ⁶⁹ The Maury Lewin Memorial Astronomical Observatory, Glendora, CA, USA
- ⁷⁰ Dept. Of Physics, University of Oxford, Denys Wilkinson Building, Keble Road, Oxford, OX1 3RH, UK
- ⁷¹ Space Exploration Sector, JHU-APL, 11100 Johns Hopkins Road, Laurel, MD 20723, USA
- ⁷² Observatoire de Strasbourg, 11, rue de l'Université, F-67000, Strasbourg, France
- ⁷³ Alain-American Association of Variable Star Observers, Le Cannet, France
- ⁷⁴ Caliche Observatory, Pontotoc, TX, USA
- ⁷⁵ NASA Jet Propulsion Laboratory, California Institute of Technology, 4800 Oak Grove Drive, Pasadena, CA 91109, USA
- ⁷⁶ Département de physique and Observatoire du Mont-Mégantic, Université de Montréal, Montréal, QC H3C 3J7, Canada
- ⁷⁷ Institute for Research on Exoplanets, Université de Montréal, Montréal, QC H3C 3J7, Canada
- ⁷⁸ Department of Astronomy, Columbia University, 550 West 120th Street, New York, NY 10027, USA
- ⁷⁹ Department of Physics and Astronomy, 12 Physics Hall, Iowa State University, Ames, IA 50011, USA
- ⁸⁰ NASA Jet Propulsion Laboratory, California Institute of Technology, 4800 Oak Grove Drive, MS 183-301, Pasadena, CA 91109, USA
- ⁸¹ Society of Astronomical Sciences, USA
- ⁸² Institut de Ciències de l'Espai (IEEC-CSIC), Carrer de Can Magrans s/n, E-08193 Barcelona, Spain
- ⁸³ Astronomy Department, University of Washington, Seattle, WA 98195, USA
- ⁸⁴ College of Life and Physical Sciences, Tennessee State University, Nashville, TN 37209, USA
- ⁸⁵ Caltech/IPAC, Pasadena, CA 91125, USA
- ⁸⁶ Ballyhoura Observatory, Ireland
- ⁸⁷ Department of Physics, Saint Michael's College, One Winooski Park, Colchester, VT 05439, USA
- ⁸⁸ Aix Marseille Univ, CNRS, LAM, Laboratoire d'Astrophysique de Marseille, Marseille, France
- ⁸⁹ Department of Physics and Astronomy, Louisiana State University, Baton Rouge, LA 70803, USA
- ⁹⁰ BAA Variable Star Section, UK
- ⁹¹ Department of Physics, Faculty of Natural Sciences, University of Haifa, Haifa 31905, Israel
- ⁹² Haifa Research Center for Theoretical Physics and Astrophysics, Haifa 31905, Israel
- ⁹³ Astronomy Department and Van Vleck Observatory, Wesleyan University, Middletown, CT 06459, USA
- ⁹⁴ Allen Telescope Array, Hat Creek Radio Observatory, 43321 Bidwell Road, Hat Creek, CA 96040, USA
- ⁹⁵ SETI Institute, 189 Bernardo, Mountain View, CA 94043, USA
- ⁹⁶ Koninklijke Sterrenwacht van België, Ringlaan 3, B-1180 Brussels, Belgium
- ⁹⁷ Institute of Astronomy, KU Leuven, Celestijnenlaan 200D, B-3001 Leuven, Belgium
- ⁹⁸ The Pennsylvania State University, 525 Davey Lab, University Park, PA 16801 USA
- ⁹⁹ University of California, Berkeley, USA
- ¹⁰⁰ Radboud University, The Netherlands
- ¹⁰¹ SETI Institute, Mountain View, CA, USA
- ¹⁰² Center for Astrophysics and Space Sciences (CASS), Department of Physics, University of California, San Diego, CA 92093, USA

- ¹⁰³ Observatories of the Carnegie Institution for Science, 813 Santa Barbara Street, Pasadena, CA 91101, USA
¹⁰⁴ Department of Physics, University of Cincinnati, Cincinnati, OH 45221, USA
¹⁰⁵ Center for Extrasolar Planetary Systems, Space Science Institute, 4750 Walnut Street, Suite 205, Boulder, CO 80301, USA
¹⁰⁶ DeKalb Observatory, MPC H63, Auburn, IN, 46706, USA
¹⁰⁷ Sierra Remote Observatories, 44325 Alder Heights Road, Auberry, CA 93602, USA
¹⁰⁸ Las Cumbres Observatory, Suite 102, 6740 Cortona Drive, Goleta, CA 93117, USA
¹⁰⁹ Clayhole Observatory, Jokela, Finland
¹¹⁰ ELTE Eötvös Loránd University, Gothard Astrophysical Observatory, Szombathely, Hungary
¹¹¹ Department of Optics and Quantum Electronics, University of Szeged, H-6720 Szeged, Dom ter 9, Hungary
¹¹² Mississippi State University, Department of Physics & Astronomy, Hilbun Hall, Starkville, MS 39762, USA
¹¹³ Hungarian Astronomical Association, Budapest, Hungary
¹¹⁴ School of Physics & Astronomy, University of Birmingham, Edgbaston, Birmingham B15 2TT, UK
¹¹⁵ Department of Astronomy, University of Virginia, Charlottesville, VA 22904, USA
¹¹⁶ Kysuce Observatory, Slovak Republic
¹¹⁷ Center for Mathematical Plasma Astrophysics, University of Leuven, Belgium
¹¹⁸ Department of Astronomy, The University of Texas at Austin, 2515 Speedway, Stop C1400, Austin, TX 78712, USA
¹¹⁹ Lowell Observatory, Flagstaff, AZ 86001, USA
¹²⁰ Astrophysics Research Centre, School of Mathematics and Physics, Queen’s University Belfast, BT7 1NN, Belfast, UK
¹²¹ Bundesdeutsche Arbeitsgemeinschaft für veränderliche Sterne, Germany
¹²² Institute of Astronomy, University of Cambridge, Madingley Road, Cambridge CB3 0HA, UK
- Received 2017 November 28; revised 2017 December 22; accepted 2017 December 22; published 2018 January 19

Abstract

We present a photometric detection of the first brightness dips of the unique variable star KIC 8462852 since the end of the *Kepler* space mission in 2013 May. Our regular photometric surveillance started in 2015 October, and a sequence of dipping began in 2017 May continuing on through the end of 2017, when the star was no longer visible from Earth. We distinguish four main 1%–2.5% dips, named “*Elsie*,” “*Celeste*,” “*Skara Brae*,” and “*Angkor*,” which persist on timescales from several days to weeks. Our main results so far are as follows: (i) there are no apparent changes of the stellar spectrum or polarization during the dips and (ii) the multiband photometry of the dips shows differential reddening favoring non-gray extinction. Therefore, our data are inconsistent with dip models that invoke optically thick material, but rather they are in-line with predictions for an occulter consisting primarily of ordinary dust, where much of the material must be optically thin with a size scale $\ll 1 \mu\text{m}$, and may also be consistent with models invoking variations intrinsic to the stellar photosphere. Notably, our data do not place constraints on the color of the longer-term “secular” dimming, which may be caused by independent processes, or probe different regimes of a single process.

Key words: comets: general – stars: activity – stars: individual (KIC 8462852) – stars: peculiar

1. Introduction

The Planet Hunters citizen science project announced the serendipitous discovery of KIC 8462852, a peculiar variable star observed by the NASA *Kepler* mission (Borucki et al. 2010) from 2009 to 2013 (Boyajian et al. 2016). KIC 8462852’s variability manifests itself as asymmetric drops in brightness of up to 22%, many of which last several days (the “dips”). There is little or no sign of periodicity in the four years of *Kepler* observations (but see Kiefer et al. 2017). Additionally, the duty cycle of the dips is low, occurring for less than 5% of the four-year period *Kepler* observed it. Subsequent ground-based follow-up observations to better characterize the star revealed nothing other than KIC 8462852 being an ordinary, main-sequence F3 star: no peculiar spectral lines, Doppler shifts indicative of orbiting companions, or signs of youth such as an infrared excess (Lisse et al. 2015; Marengo et al. 2015; Boyajian et al. 2016; Thompson et al. 2016).

In addition to the short-term variability seen in the *Kepler* long-cadence data, Schaefer (2016) discovered a variable

secular decline averaging 0.164 ± 0.013 mag per century in archival data taken from 1890 to 1989. While Hippke et al. (2016) claim the dimming found by Schaefer (2016) is spurious, the unique longer-term variability was again identified with the *Kepler* full-frame images, which show that KIC 8462852 underwent secular dimming by a total of 3% during the four-year (2009–2013) *Kepler* time baseline (Montet & Simon 2016). More recently, Meng et al. (2017) presented over 15 months of space- and ground-based photometry from *Swift*, *Spitzer*, and *AstroLAB IRIS*, showing that this variability continues even today. Further results from ground-based data over 27 months with *ASAS-SN* data, and from 2006 to 2017 with *ASAS* data also confirm such dimmings, with possible signs of periodic behavior (Simon et al. 2017). Thus, KIC 8462852 is known to display complex dip-like variations with a continuum of duration timescales ranging from a day to a week to a month to a year to a decade to a century.

Wright & Sigurdsson (2016) re-evaluated the landscape of families of possible solutions that would be consistent with not only the complex dipping patterns, but also the long-term secular dimming. These included broad categories of solutions such as those invoking occulting material in the solar system, material in the interstellar medium (ISM) or orbiting an intervening compact object, circumstellar material, and variations intrinsic to the star. Specific models for the brightness variations have been explored by Katz (2017), who modeled a

¹²³ NASA Postdoctoral Program Fellow, Nexus for Exoplanet System Science.

¹²⁴ NSF Astronomy and Astrophysics Postdoctoral Fellow.

¹²⁵ Miller Senior Fellow, Miller Institute for Basic Research in Science, University of California, Berkeley, CA 94720-3411.

¹²⁶ Einstein Fellow.

¹²⁷ PI, Nexus for Exoplanet System Science.

circumstellar ring; Makarov & Goldin (2016), who suggested interstellar “comets”; giant circumstellar exocomets, suggested by Boyajian et al. (2016) and modeled by Bodman & Quillen (2016); Neslušan & Budaj (2017), who modeled dust clouds associated with a smaller number of more massive bodies; Ballesteros et al. (2018), who suggested a ringed planet and associated Trojan asteroid swarms; Sheikh et al. (2016), who find the statistics of the dips to be consistent with intrinsic processes; Metzger et al. (2017), who model the consumption of a secondary body; and Foukal (2017a), who invoke intrinsic variations perhaps related to magnetocvection.

Recently, Wyatt et al. (2018) showed that both the dips and dimming could be compatible with circumstellar material distributed unevenly along an elliptical orbit. These results advocate for additional tests with the various proposed circumstellar scenarios in order to resolve whether the dynamical history of such material could produce the shapes of the dips.

After the end of the *Kepler* prime mission, we initiated a ground-based monitoring program in order to catch a dimming event in nearly real time. This paper focuses on the first dip in the *Elsie* family, and future papers will focus on the dips that follow. In Section 2, we describe the observations of the first ground-based detection of a dimming event in KIC 8462852. We present several first results from the photometric, spectroscopic, and spectropolarimetric analysis in Sections 3 and 4, and conclude by describing future work.

2. Observations

2.1. Time-series Photometry

KIC 8462852 is a northern hemisphere target ($\delta = +44^\circ$) with $V = 11.7$ mag. From May to September, the star is typically available above airmass 2 for ~ 4 – 8 hr at northern hemisphere observatories, with a decreasing window of visibility until the end of December. In this paper, we present photometric data from several observatories, as described briefly here and in the Appendix.

Regular photometric monitoring in multiple filters of KIC 8462852 started in 2016 March with the Las Cumbres Observatory (LCOGT) 0.4 m telescope network, which consists of telescopes at two northern hemisphere sites: TFN (Canary Islands, Spain) and OGG (Hawaii, USA).¹²⁸ On JD 2,457,892 (UT 2017 May 18; UT dates are used throughout this paper), a drop in brightness was claimed as significant from both TFN and OGG measurements. Observations acquired at Fairborn Observatory corroborated this drop in brightness, and an alert for triggered observations was immediately executed. In response to the alert, we acquired additional photometric observations from the Calvin, Master-II, Wise, Joan Oró (TJO), Trappist-N, Thatcher, NITES, and Gran Telescopio Canarias (GTC) telescopes. We showcase this first event observed in 2017 May (“*Elsie*”; Section 2.1.1) observed by each observatory in Figure 1, each point of the time series being a nightly average of the differential magnitude in the specified band. Since most observatories did not have monitoring before the event, we normalize each data set assuming that the stellar flux was at the “true” stellar level just after the first event (JD 2,457,900) to ensure consistency. Note that the analysis

carried out in Section 3.1 to determine colors of the dip uses the LCOGT data sets. These data are normalized using before dip data where the longer baseline improves the normalization (details in Section 3.1).

2.1.1. The *Elsie* Dip Family

In Figure 2, we show the full LCOGT 0.4 m time series from 2017 May through December in the r' band. The LCOGT observations are a product of a successful crowd-funding effort through Kickstarter.¹²⁹ As a part of the campaign’s design, those who supported the project were eligible to nominate and then vote on the name of the dips. Four major dipping events happened over this time period. The first, which we named “*Elsie*,”¹³⁰ reaches a minimum around UT 2017 May 19 (JD 2,457,893). Its full duration spans the course of ~ 5 days. The temporal gradient of the dip ingress is much sharper than the egress, where the recovery appears to hesitate, making an asymmetric profile overall. Hereafter, we refer to the full period of variability observed in 2017 as the *Elsie* dip family.

A few weeks after the end of *Elsie*, the second event, “*Celeste*,”¹³¹ began to make an appearance, reaching its deepest point around UT 2017 June 18 (JD 2,457,922). *Celeste* lasted for a couple of weeks, having a slow decline to its minimum, but then a much more rapid post-minimum rise up. The rapid egress was stunted about two-thirds of the way up, however, and the flux remained $\sim 0.5\%$ below normal brightness levels. This 30-day-long depression after *Celeste* was never given a name, since it was unsubstantial compared to the first two events. We do, however, identify this region to be a statistically significant detection of a $\sim 0.5\%$ decrease in brightness, which was also independently observed at several other observatories (E. Bodman et al. 2018, in preparation).

The third event, “*Skara Brae*,”¹³² began to appear just when the month-long depression after *Celeste* showed possible signs of recovery. *Skara Brae* behaved very similarly to *Celeste* in a mirror-image profile, with a $\sim 1\%$ depth in r' -band lasting on the order of two weeks. In the middle of *Skara Brae* (on UT 2017 August 8; JD 2,457,974) there was an additional narrow (few hour) $\sim 2\%$ dip. We did not observe the ingress of this dip (which could have lasted up to 7 hr) because this region fell within a gap between observatories, but observations from both LCOGT and TJO caught the rapid return to the level of the broad dip over a 4 hr period. This event was the first and only significant short-timescale (< 1 day) variability observed in the 2017 *Elsie* family of dips (Figure 2, open circles). We show a close-up of this feature in Figure 3. While this is a seemingly drastic change in brightness within the *Elsie* family, we find that the dip

¹²⁹ <https://www.kickstarter.com/projects/608159144/the-most-mysterious-star-in-the-galaxy>

¹³⁰ The name *Elsie* is a play on words with “L + C,” short for “light curve,” and is also a wink and a nod to the “L” as “C” umbrae Observatory, for making the project happen.

¹³¹ This dip [first] appeared to have a slow decline with a quick rise, which is close to a mirror image of *Elsie*, which had a quick decline with a slow rise. *Elsie* (or “LC”) in reverse is “CL” or “ciel,” which means “sky” or “heavenly” in French. “*Celeste*” is the original Latin name from which “ciel” is derived.

¹³² The brightness variations for KIC 8462852 share some of the same traits as this lost city located in the far north of Scotland. They are ancient; we are watching things that happened more than 1000 years ago. They are almost certainly caused by something ordinary, at least on a cosmic scale. And yet that makes them more interesting, not less. But most of all, they are mysterious. What was going on there all those centuries ago?

¹²⁸ In 2017 November, an additional northern hemisphere site, ELP (Texas, USA), was added to the LCO network.

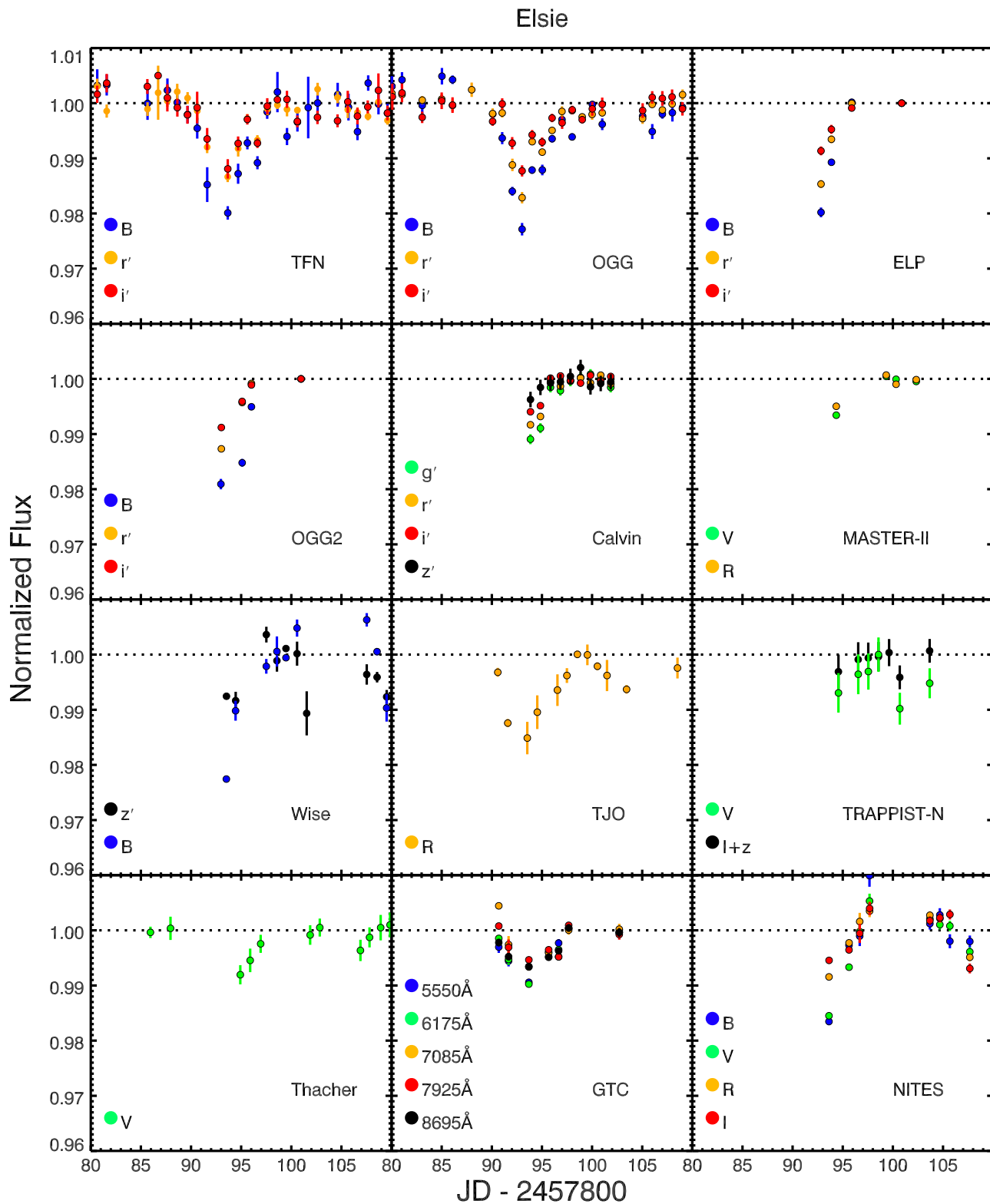


Figure 1. Time-series photometry of *Elsie*. See legends for observatory and filter information, and Section 2.1 for details.

gradient here ($\sim 0.2\% \text{ hr}^{-1}$, or $\sim 5\% \text{ day}^{-1}$) is not extreme compared to the dip gradients observed by *Kepler*, which can be up to a factor of 10 steeper (Boyajian et al. 2016).

This smaller gradient could indicate that the current dips are less optically thick than those with steeper gradients by *Kepler*, which would be consistent with the smaller dip depths,

although other geometric factors may also play a role. In any case, the *Kepler* observations still provide the most stringent constraint on the orbit of the parent body (or bodies) from consideration of the light-curve gradient (Boyajian et al. 2016). We also find that the duration of this event is no shorter than the shortest seen by *Kepler*, which was 0.4 days. Finally, we

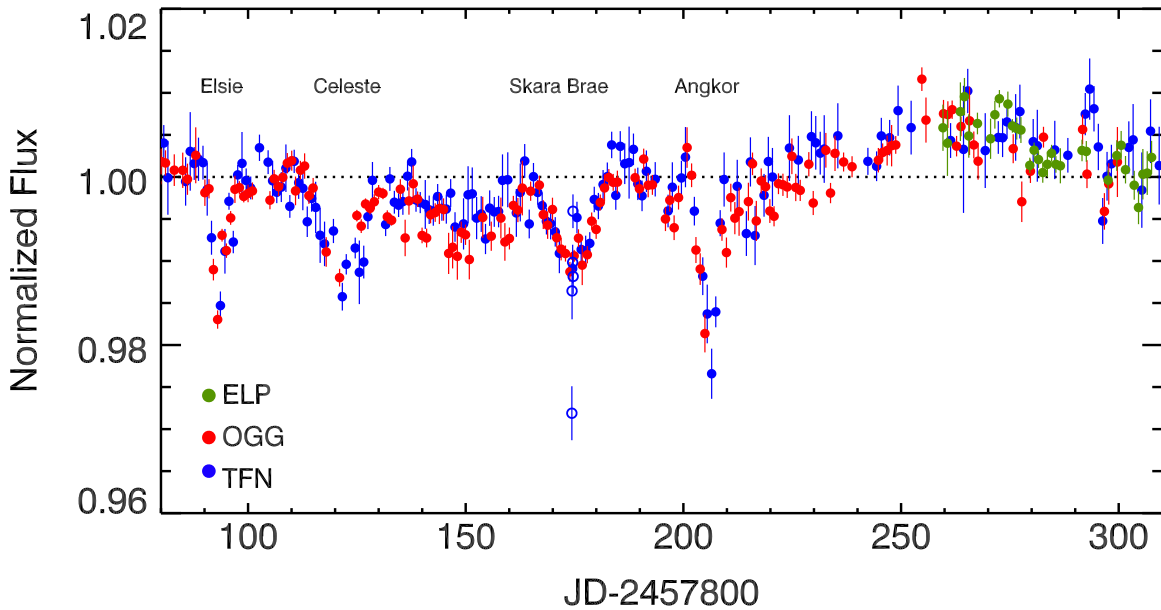


Figure 2. LCOGT time-series photometry of KIC 8462852 in the r' band from 2017 May through December showing the *Elsie* dip family. Each point is a daily average from the LCOGT 0.4 m stations indicated in the legend. Near the midpoint of *Skara Brae*, short-term variability seen over a few hours is indicated as open blue points (see also Figure 3). For details, see Sections 2.1 and 2.1.1.

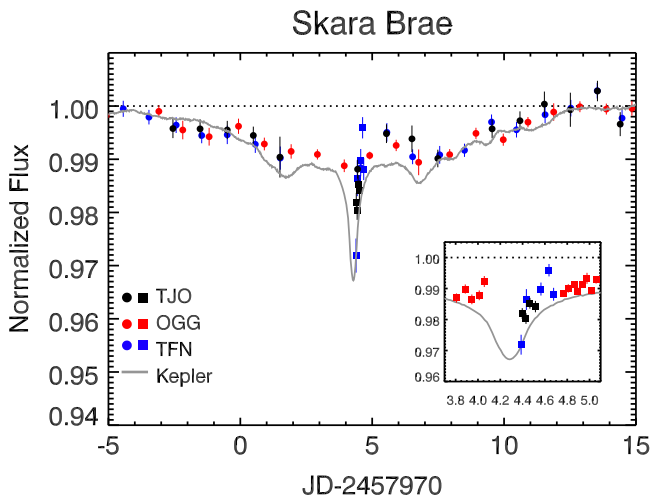


Figure 3. *Skara Brae* event showing daily averages (circles) of ground-based measurements. The solid gray line depicts the *Kepler* long-cadence data from D1540 shifted in time to illustrate the similarity between the events. Near the midpoint of *Skara Brae*, we show the hourly averages (squares) from LCOGT and TJO to illustrate the short-term variability seen over a span of a few hours. The plot inset is a close-up view of this midpoint region. See Section 2.1.1 for details.

note that *Skara Brae*'s full contour—a symmetrical broad shallow dip containing a brief deep dip within—is unique.¹³³ This allows us to compare its appearance with the dips observed by *Kepler*, where only a couple were at a similar level of 1%–2%. We find the *Kepler* dip at D1540 (Boyajian et al. 2016) being remarkably similar in depth, shape, and duration (see Figure 3 for a direct comparison).

“*Angkor*,”¹³⁴ the fourth significant dip in the complex, appeared two weeks after *Skara Brae*, reaching its deepest

depth around UT 2017 September 9 (\sim JD 2,458,006). The *Angkor* ingress exhibited the most rapid, sustained (\sim 4 days long) flux gradient observed for the star from the ground to date, and the egress was similarly rapid, though it remained at a depth of \sim 0.5% below normal for about a week before brightening to slightly above normal levels. The post-*Angkor* monitoring data rose up \sim 0.5% compared to pre-*Elsie* levels (dotted line, Figure 2). Around the end of 2017 October (JD 2,458,050) this brightening trend reversed, returning back to unity by mid-December (\sim JD 2,458,100).

2.2. Spectroscopy

Over a six-month period, beginning 2017 May 20, we acquired low-resolution spectra with the Kast Double Spectrograph, mounted on the 3 m Shane telescope (Miller & Stone 2013) at the Lick Observatory, as well as from the DEep Imaging Multi-Object Spectrograph (DEIMOS; Faber et al. 2003) and the Low Resolution Imaging Spectrometer (LRIS) using the Keck telescopes. All of the Lick and Keck low-resolution spectra are broadly consistent with the object being a main-sequence F star; a future paper will present them in greater detail (M. Martínez González 2018, in preparation). A total of eight high-resolution spectra were acquired with the HIRES spectrograph on Keck I. Five of the eight were taken prior (circa 2015, 2016), and the other three were taken during the *Elsie* event. First, we checked for radial velocity (RV) variations. We fine-tuned the wavelength solution using the numerous telluric lines in the vicinity of Na I D using the telluric spectrum from the Wallace et al. (2011) solar atlas, applied barycentric velocity corrections calculated with the IDL code BARYCORR (Wright & Eastman 2014), verified that the ISM lines remained fixed, and measured RV offsets between each out of dip spectrum along with their coadded average and the three in-dip spectra, resulting in $\Delta RV = 0.38 \pm 0.35 \text{ km s}^{-1}$. We are unable to discern RV variability with the present quality of the wavelength solutions during these

¹³³ “Think of the dip’s creator being something like a giant Jupiter-sized kernel of corn, that halfway across the star pops into a *popjupitercorn*, for maybe a few hours, then spontaneously de-pops.”—T. Hicks; 2017 August.

¹³⁴ Following the theme of lost cities, *Angkor* is perhaps the greatest lost city of medieval times.

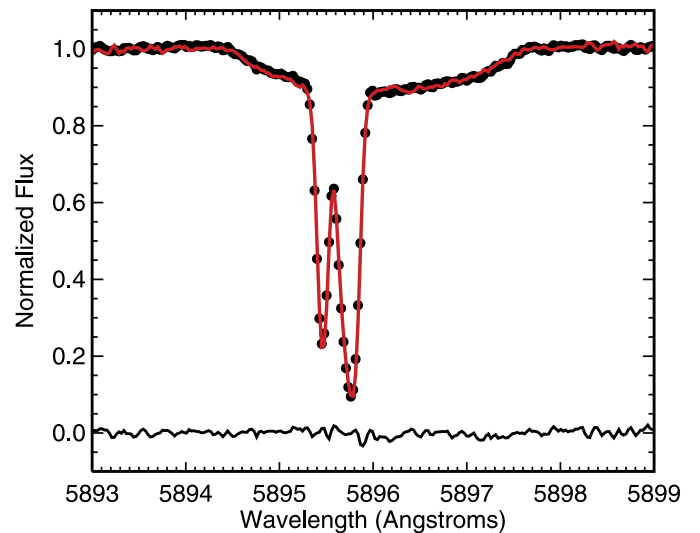
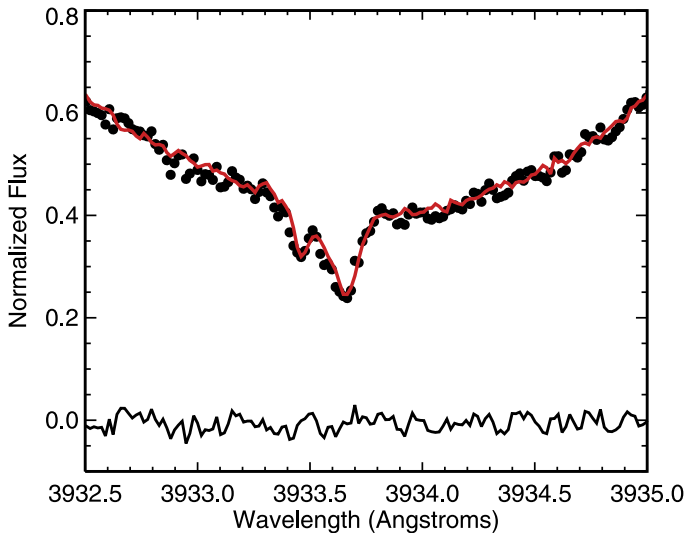


Figure 4. Hires spectra of KIC 8462852 at the Ca II K (left) and Na I D1 (right) lines prior to (black dots) and during (red line) the *Elsie* event, along with residuals (prior minus during). Error bars are smaller than the black symbols. We measure no significant variation in stellar RV ($\Delta < 0.4 \text{ km s}^{-1}$) or equivalent width of the ISM lines ($< 1\%$), as evidenced by the residuals. See Section 2.2 for details.

epochs, limiting the presence of anything larger than a gas giant within 0.1 au.

The ISM imprints absorption lines in spectra at Ca II (H and K at 3968.469 Å and 3933.663 Å), Na I (D2 at 5889.951 Å, D1 at 5895.924 Å), and K I (7698.964 Å); unfortunately, our in-dip spectra do not reach K I. Close-up views of the Ca II K and Na I D1 spectral regions are shown in Figure 4, along with their residuals (prior minus during *Elsie*). The foreground ISM can be described by three Gaussians (the profile of the redder of the two apparent components is asymmetric and is clearly blended with at least one additional component). We find no significant variations in the depths of these ISM lines (i.e., differences in equivalent widths of the ISM lines are $< 1\%$), following the procedures outlined by Wright & Sigurðsson (2016) and Curtis (2017). The amplitude of the residuals at these ISM lines is on par with variability due to the S/N, and it will be challenging to discern real changes in interstellar absorption at or below this level during future events without higher-quality spectra (or larger dips).

2.3. Infrared Photometry

NEOWISE observations of KIC 8462852 in the W1 (3.4 μm) and W2 (4.6 μm) bands were acquired a week before *Elsie*, and serendipitously on JD 2,457,892 (around the time of the largest optical flux decrease for *Elsie*) with the spacecraft’s occasional toggle to avoid the Moon. All NEOWISE observations of KIC 8462852 were extracted without any cuts on flag parameters. Inspecting each detection, we see that all observations had ph_qual ratings of “A” in both bands, and none of the detections were affected by latent images, other persistence features, or diffraction spikes as would be indicated by the “cflags” parameter (Cutri et al. 2015). We show this temporal series in Figure 5. We find no detectable change in brightness with the observations taken during *Elsie* compared to the week prior in either of the NEOWISE bands. Work is currently underway analyzing near-IR measurements (D. Clemens et al. 2018, in preparation) and additional mid-IR measurements (H. Y. A. Meng et al. 2018, in preparation) taken throughout the *Elsie* family of dips to put additional constraints on variability after this first event.

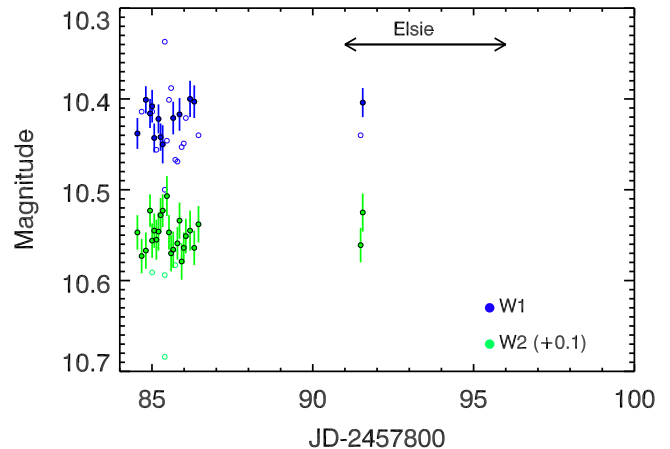


Figure 5. NEOWISE time-series photometry of KIC 8462852 in the W1 (3.4 μm) and W2 (4.6 μm) bands according to the legend at the bottom right. Measurements with the PSF-fitting quality metric $\chi^2_{\text{PSF}} < 2$ are shown as filled points with their associated 1σ uncertainties; otherwise, the point is unfilled and without uncertainties for clarity. The approximate timing of *Elsie* identified in optical data is marked on the graph. See Section 2.3 for details.

2.4. Polarimetry

Evidence for the scattering of stellar light by circumstellar dust can be probed with polarimetry. Spectropolarimetry of KIC 8462852 was obtained with the Kast spectropolarimeter on the 3 m Shane reflector at the Lick Observatory (see Mauerhan et al. 2014 for a description of the Kast instrument) at eight epochs: 2017 May 20.4; June 2.3, 21.4, 27.4; July 1.4, 16.4, 17.4; and August 1.4. On each night, the source was observed 18 minutes for each Stokes parameter Q and U , for a total of 36 minutes on-source integration time. The polarization P and position angle θ were derived according to the methodology described by Mauerhan et al. (2014). On every night, two strongly polarized standard stars (Hiltner 960 and HD 204827) and one weakly polarized star (HD 212311) were observed for calibration purposes. HD 204827, in particular, was used to calibrate the position angle on the sky.

Over the course of our eight epochs, KIC 8462852 exhibited an average (standard deviation) polarization of $P = 0.46(0.05)\%$

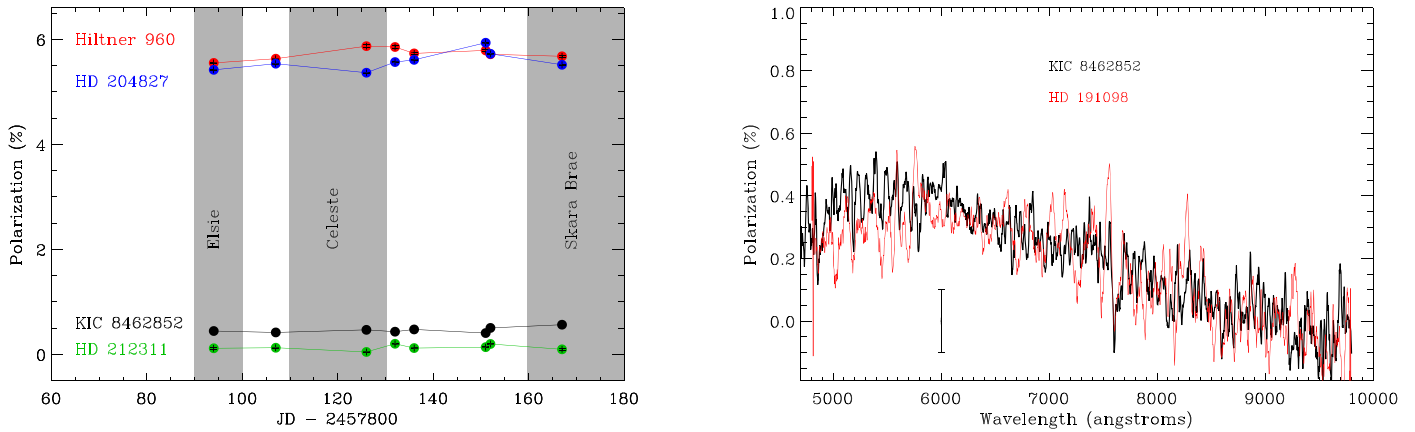


Figure 6. Left: polarization over time for KIC 8462852 (black), Hiltner 960 (red), HD 204827 (blue), and HD 212311 (green). The statistical uncertainties appear smaller than the data points. Right: polarization and position-angle spectra of KIC 8462852 (black curve). The data are the average of all seven epochs of observations performed in 2017 May–August. The red curve represents data for a nearby star HD 191098, which was used as a probe of interstellar polarization. The noise fluctuations of KIC 8462852 reflect the total statistical and systematic measurement uncertainty, which we estimate at $\pm 0.10\%$ (graphically represented near bottom center). See Section 2.4 for details.

and position angle $\theta = 91.0(2.6)$ in the V band (5050–5950 Å). The statistical uncertainty in P was typically 0.01% on a given epoch, but in our experience with Kast the systematic uncertainties are usually at least 0.1%–0.15%. Over the same period, the average (standard deviation) V -band polarization of our polarized standard Hiltner 960 is $P = 5.58(0.18)\%$, $\theta = 54.9(0.7)$, consistent with published values (Schmidt et al. 1992). The weakly polarized star HD 212311 exhibited $P = 0.13(0.05)\%$, within 2σ of the Schmidt et al. (1992) value. The results are illustrated in Figure 6, and indicate that KIC 8462852 did not vary significantly in polarization, relative to our calibration stars.

The polarization characteristics of KIC 8462852 appear to be consistent with interstellar polarization, presumably induced by the dichroic absorption of light by nonspherical dust grains oriented along the Galactic magnetic field. Figure 6 illustrates the polarization and position-angle spectra of the source, along with the F5 V star HD 191098 ($V = 10.09$ mag; 0.2° from KIC 8462852 on the sky), which we used as a probe of the approximate interstellar polarization on 2017 June 2; the spectroscopic parallax distance of this star ($M_V = 3.5$ mag) is ~ 201 pc, which is not ideal, since KIC 8462852 lies at a much greater estimated distance of 391 pc. Nonetheless, HD 191098 can provide a useful probing of interstellar polarization if the majority of intervening material is closer to Earth than both sources. The spectropolarimetric data for both KIC 8462852 and HD 191098 follow the wavelength-dependent “Serkowski” form Serkowski et al. (1975) that is expected for interstellar polarization from Galactic dust (where the peak polarization is typically seen near 5300–5400 Å). HD 191098 exhibits a V -band polarization of $P \approx 0.40\%$, $\theta \approx 78^\circ$, only slightly lower than that of KIC 8462852 in magnitude and offset by $\sim 14^\circ$ in position angle. Moreover, we examined the polarization of three stars from the catalog of Heiles (2000) that lie within 2° of KIC 8462852 on the sky: HD 190149, HD 191423, and HD 191546. The average (standard deviation) polarization and position angle exhibited by these stars is $P = 0.47(0.36)\%$ and $113^\circ(18^\circ)$. This is also comparable to our measurements of KIC 8462852.

The polarization we measure appears to be significantly lower than the broadband imaging polarimetry values that Steele et al. (2018) have reported with the RINGO3 instrument (Słowikowska

et al. 2016) over a similar time period. For example, over 2017 May through August, they reported a nonvariable source ($< 0.2\%$ fluctuation) with average polarization and position angle of $P = 1.2\%(0.2\%)$, $\theta = 72^\circ(6^\circ)$ for the b^* band (3500–6400 Å); $P = 0.6\%(0.1\%)$, $\theta = 74^\circ(6^\circ)$ for the g^* band (6500–7600 Å); and $P = 0.6\%(0.1\%)$, $\theta = 73^\circ(6^\circ)$ for the r^* band (7700–10000 Å). However, the level of discrepancy between these measurements and ours is not particularly surprising, given the large systematic uncertainties associated with the RINGO3 instrument (Słowikowska et al. 2016). Regardless of systematics, we reiterate that the results here and those from Steele et al. (2018) both show that the object has polarization properties typical of its location on the sky, and limit any change in optical polarization between in and out of dip epochs of $< 0.05\%$ (Kast) and $< 0.1\%$ – 0.2% (RINGO3). Finally, we note that analyses of near-IR polarimetry taken during the *Celeste* event are underway and should be able to provide additional constraints for the system and its environment (D. Clemens et al. 2018, in preparation).

2.5. Radio SETI

The Allen Telescope (SETI Institute) performed a series of KIC 8462852 radio observations during the *Elsie* dimming event. These were subsequent to the observations in 2015 (Harp et al. 2016). From 2017 July 8 through August 8, 1022 separate 92 s observations were performed that resulted in scanning 1419–4303 MHz for radio signals. No narrowband radio signals were found at a level of 180–300 Jy in a 1 Hz channel, or medium-band signals above 10 Jy in a 100 kHz channel, which would correspond to transmitters at the distance of KIC 8462852 having effective isotropic radiated power (EIRP) of $(4\text{--}7) \times 10^{15}$ W and 10^{19} W for the narrowband and moderate-band observations. While orders of magnitude more powerful than the planetary radar transmitter at Arecibo Observatory, 2×10^{13} W EIRP, the actual power requirements would be greatly reduced if emissions were beamed directly at Earth.

3. Analysis

3.1. Size, Shape, and Wavelength Dependence of *Elsie*

In the discussion presented here, we limit the range of our analysis to the first event, *Elsie*; the analysis of the remaining *Elsie* dip family will be presented by E. Bodman et al. (2018, in

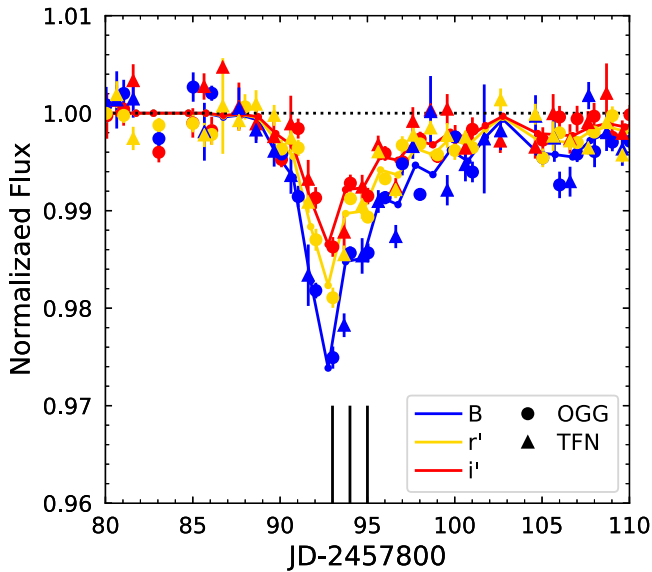


Figure 7. Plot of the *Elsie* dip with $N + 8$ model fit. Red, yellow, and blue indicate i' , r' , and B filters (respectively) for the data points and fit lines. The different observatory sites are indicated by different marker shapes as depicted in the legend, and each data point is the average daily value. Our fit results in the depth ratios of *Elsie* to be $B/i' = 1.94 \pm 0.06$ and $r'/i' = 1.31 \pm 0.04$. See Section 3.1 for details. The black vertical lines indicate when Keck/HIRES spectra were taken (see Section 2.2).

preparation). We also assume that the differential fluxes found in each filter are measures of the additional opacity causing the dips, not the total color of all the material along the line of sight (i.e., we apply no correction in the baseline flux for the longer-term brightness variations). For the following discussion, we define depth ratios, B/i' and r'/i' , as the ratio of the dip depths measured in normalized flux in the B to i' filters and r' to i' filters, respectively.

Continuous time-series coverage throughout the *Elsie* event shows the largest depth of 2.5% in the B band on JD 2,557,893. With monitoring across the many observatories, we obtained a nearly continuous cadence time series during *Elsie*, and thus can rule out a missed detection of a deep, short-lived dip, with the longest data gap occurring daily from 15 to 19 UT (a duration of ~ 0.2 days). We fit the LCOGT multiband light curve with an $N + 8$ parameter model, where N is the number of days over which the fitted data are taken. The unbinned data for each site are used for the fit.

A single depth ratio for each filter set (B/i' and r'/i') is assumed for the entire dip. We include normalizations (n) of each telescope in each filter as free parameters, resulting in a total of six normalizations, to ensure that the different sites are normalized in a consistent manner. Each day has a depth (d_i) in the i' filter fit to the data binned in that day. When d_i is fit, it is compared to the i' band for each applicable site with normalization, and to the B and r' data after multiplied by the depth ratio (R) and normalization, e.g., $F_{\text{Filter}} = n_{\text{Filter}}(1 - d_i \times R_{\text{Filter}})$. This allows for the color ratios, the normalizations, and the depths to be fit simultaneously. In order to prevent the normalizations from wandering too far from 1.0, we include 10 days of pre-*Elsie* data, where the depths are set to 0. To overcome degeneracies in the fit, we explored the parameter space with the Markov Chain Monte Carlo method using the “emcee” package (Foreman-Mackey et al. 2013). We used flat priors over ranges 0.5–5, 0.99–1.01, and 0–0.2 for the depth ratios,

normalizations, and depths (respectively), with the results of a least-squares fit as the starting point. The results of the Bayesian fit are shown in Figure 7, and the depth ratios are $B/i' = 1.94 \pm 0.06$ and $r'/i' = 1.31 \pm 0.04$. The r'/i' ratio measured at the Calvin Observatory (1.29) is in agreement with the LCOGT value. The extinction due to optically thin dust is typically characterized by a higher extinction at bluer wavelengths such as is observed for KIC 8462852 during the *Elsie* dip. The ratios observed indicate dust grain sizes larger than are seen for interstellar dust and are more likely to arise from circumstellar dust (Savage & Mathis 1979; Meng et al. 2017).

3.2. Particle Size and Chemical Composition

Under the assumption that the dimming is caused by intervening dust, the multicolor observations taken during *Elsie* may be used to put some constraints on the particle size and chemical composition. We therefore compared the measured amount of attenuation in different filters found in the previous section, $B/i' = 1.94 \pm 0.06$ and $r'/i' = 1.31 \pm 0.04$, with the theoretical ratios of dust opacities for optically thin distributions at those wavelengths. The opacities of grains for different chemical compositions and different particle sizes are taken from the tables of Budaj et al. (2015). These opacities assume homogeneous spherical dust grains with a relatively narrow Deirmendjian particle size distribution (FWHM ≈ 0.4 dex; Deirmendjian 1964), as well as effective wavelengths of B , r' , and i' of 0.4361, 0.6215, and 0.7545 μm , respectively. We explore the signatures of a few refractory dust species and water ice. Silicates are perhaps the most important refractory species. They are divided into the family of pyroxenes and olivines. Optical properties of silicates are quite sensitive to the amount of iron in the mineral and that is why we explore iron free and iron rich cases. Namely, for pyroxenes ($\text{Mg}_x\text{Fe}_{1-x}\text{SiO}_3$), we consider the two cases: a mineral with zero iron content ($x = 1$), which is called enstatite and a pyroxene with 60/40 iron/magnesium ratio. The refractive indexes of these pyroxenes are taken from Dorschner et al. (1995). Olivines ($\text{Mg}_{2y}\text{Fe}_{2-2y}\text{SiO}_4$) may also have different iron content. Again we consider the mineral with zero iron content ($y = 1$) called forsterite, and use its refractive index from Jäger et al. (2003). We also consider an olivine with 50/50 iron to magnesium ratio, taking its index of refraction from Dorschner et al. (1995). Alumina (Al_2O_3) is one of the most refractory species, which might be present in such environments and we take the complex refractive index for γ alumina from Koike et al. (1995). The refractive index for iron is taken from Johnson & Christy (1974). Those of carbon are from Jager et al. (1998), and they assume carbon at high temperature (1000 $^\circ\text{C}$). Lastly, the complex index of refraction for water ice is taken from Warren & Brandt (2008).

The comparison between the observed and theoretical opacity ratios for different modal size (i.e., radius) of the grains and their chemical composition is shown in Figure 8. We find that most of the silicates and alumina should have particle sizes of about 0.1–0.2 μm . If the dust were composed solely from iron, it would have significantly smaller particles of about 0.04–0.06 μm . Carbon would require even smaller particles, $< 0.06 \mu\text{m}$. On the other hand, water ice would require 0.2–0.3 μm particles. We conclude that regardless of composition, the dust is $\ll 1 \mu\text{m}$ in size and optically thin, which is consistent with the predictions in Figure 3 of Wyatt et al.

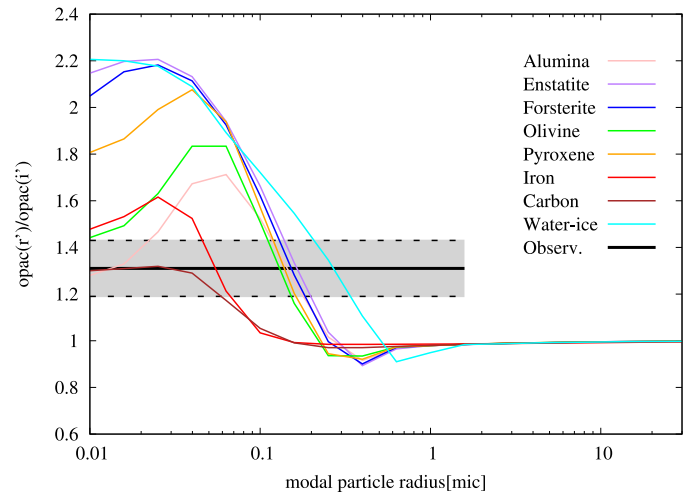
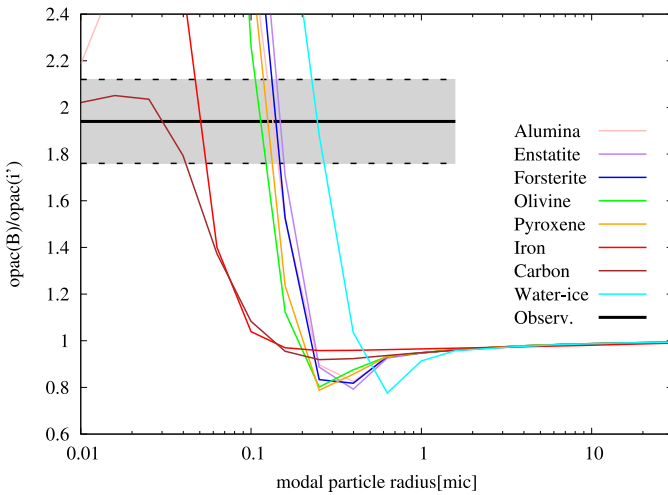


Figure 8. Opacity ratio in B/i' (left) and r'/i' as a function of modal particle radius for several dust species as indicated in the legend. Observations with 3σ limits are plotted as horizontal lines. See Section 3.2 for details.

(2018). Circumstellar dust that is this small would be strongly affected by radiation forces, putting it on an unbound orbit as soon as it was created. Thus, if it is circumstellar, the dust causing these short-duration dips must have been created recently, since radiation forces would cause it to spread from its point of origin.

4. Discussion

The detection of dips from the ground extends the duration of dip activity in KIC 8462852 from the four years of the *Kepler* mission, to eight years since the beginning of the *Kepler* mission. The complexity and duration of the *Elsie* dip family is reminiscent of the Quarter 16 (Q16) dip complex during the *Kepler* mission (see Figure 1 of Boyajian et al. 2016) and suggests that additional dip complexes may be seen in the future. While the similarity of *Skara Brae* to the *Kepler* D1540 event (Figure 3) suggests a potential periodicity for this particular event, the broader differences between the *Elsie* family of dips and the Q16 complex suggest a significant stochastic component to the dip mechanism, if it is periodic. The detection of dips from multiple independent observatories as illustrated in Figure 1 also demonstrates that they are real (i.e., astrophysical in origin), firmly ruling out an instrumental/data-reduction artifact as the source of the *Kepler* dips.

While they are far more precise, the *Kepler* observations were in a single wide bandpass, so the color dependence of the dips could be inferred only with multiwavelength observations such as those presented here. These colors provide important new constraints; in a scenario where the dips are caused by material passing between us and the star, the colors measured in Section 3 are consistent with extinction by optically thin submicron-sized dust (Figure 8; see also Figure 3 of Wyatt et al. 2018). This conclusion is in contrast to longer-term observations that suggest that the wavelength dependence of the secular dimming is less pronounced, and therefore that intervening dust should be larger (Meng et al. 2017). Thus, the current evidence suggests that the short-term and long-term dimming are caused by dust of different sizes.

This difference could be a natural consequence of models that invoke exocomets or dust-enshrouded planetesimals; the dust concentrations that cause the short dips were created recently, and are richer in small, but short-lived, dust that is

quickly ejected by radiation forces. Larger dust that is created survives and remains on a circumstellar orbit spreading from its point of origin in a manner similar to comet dust tails, causing the secular dimming. In such a scenario, we also would not expect to see the same dust causing the short-duration dips in Figure 2 to return one orbit later, although the source of the dust may return one orbit later, creating fresh dust.

If we further assume that the material is in a highly elliptical, circumstellar orbit, Wyatt et al. (2018) provide predictions to the infrared component of the dip based on several possible orbital configurations. In Section 2.3, our results show that the NEOWISE W1 and W2 measurements taken coincident with *Elsie* would rule out orbits with pericenter distances $q < 0.03$ au and $q > 0.3$ au. If *Elsie* were a deeper dip, the constraints from the mid-infrared observations would have been stronger. However, in this case, the Wyatt et al. (2018) models show that to better constrain the location of material during a 2% dip, observations taken at 10–30 μm with a future space telescope would be necessary.

Elsie's dip depth wavelength dependence constrains and challenges many proffered models for the dips. For instance, intervening opaque material (e.g., a planet or megastructure) should produce wavelength-dependent dips only to the degree that there is nonuniformity across the stellar disk, such as from limb darkening or gravity darkening. Using a Mandel & Agol (2002) model, assuming a central transit and Claret & Bloemen (2011) limb-darkening coefficients appropriate for KIC 8462852 (and assuming negligible gravity darkening, appropriate given the star's $v \sin i$ value), we find a difference of 10% between transit depths in notional filters around 4400 \AA (approximately B) and 7600 \AA (approximately i'), implying a B/i' depth ratio of ~ 1.1 , in strong disagreement with our observed values of ~ 2 (Section 3.1; Figure 7).

To explore whether the observed colors are consistent with the appearance of cool spots, we have used both blackbody and Castelli & Kurucz (2004) model spectra to compute the brightness of a star in the B and i' bands as functions of temperature T , where T_0 is the nominal effective temperature of KIC 8462852, 6720 K.¹³⁵ We calculate the depth of a dip in

¹³⁵ We use the B filter curve from Bessell (1990) and the i' filter curve from <http://www.aip.de/en/research/facilities/stella/instruments/data/sloan-griz-filter-curves>.

band X due to the temporary appearance of a spot of temperature T occupying a fraction A of the stellar surface as

$$\delta_X = \frac{X(T_0) - ((1 - A)X(T_0) + AX(T))}{X(T_0)} = A \left(1 - \frac{X(T)}{X(T_0)} \right), \quad (1)$$

where (as with the data presented here) we normalize the brightness of the star against the pre-dip brightness. The ratio of the dip depths in the B and i' bands in these models¹³⁶ is then

$$\frac{\delta_B}{\delta_{i'}} = \frac{1 - B(T)/B(T_0)}{1 - i'(T)/i'(T_0)}, \quad (2)$$

independent of spot size (this model thus includes the case of the entire photosphere changing temperature at constant radius, which is more consistent with the lack of rotational modulation of any surface features). We find that this function yields dip depth ratios of 1.86 in the case of Kurucz model atmospheres and 1.65 with a blackbody approximation. The former value is formally 1.3σ from our measured value of $B/i' = 1.94 \pm 0.06$; however, only 7% of our posterior samples had $B/i' < 1.86$. Our *Elsie* multiband photometry thus may be consistent with models in which transient cool surface regions explain the dips.¹³⁷ Note that this simple analysis does not address models invoking the disappearance of regions much hotter than T_0 , or those that invoke a changing stellar radius.

Invoking dust still challenges our creativity in developing a unified theory to explain all the observations; however, the models of Wyatt et al. (2018) give hope to a swarm of yet unspecified objects in an eccentric orbit (in this case, exocomets, with an alternative being dust-enshrouded planetesimals as proposed by Neslušan & Budaj 2017) causing the brightness fluctuations. Continued monitoring to detect events in the future will help narrow down any periodicity within the dip occurrence, which would strengthen the argument that the source of the obscuring material was in orbit around the star, as opposed to density fluctuations in the ISM, etc.

In fact, if the two deepest events in the *Kepler* data were caused by a recent planet–planet collision, Boyajian et al. (2016) predicted 2017 May to be the next event—and this was precisely when *Elsie* appeared. However, this prediction was based solely on the two large events taking place roughly two years apart (in 2011 and again in 2013), and came with several caveats. The obvious issue discussed was the low probability of witnessing such an event, given the lifetime of the *Kepler* mission, geometry, system age, and lack of any IR excess based on the timing of the *WISE* observations (circa 2010). Another issue with this prediction, however, is that it would not explain the *Kepler* dips that happened between the large events. Moreover, even though the *Elsie* family appeared timely in this prediction, the other predicted 2015 April event went undetected because no monitoring was ongoing at the time.¹³⁸ This gap in time coverage hinders any truly periodic

interpretation based on the occurrence *and* nonoccurrence of the dips.¹³⁹ Furthermore, as previously mentioned, each of the dips lack resemblance to one another, and while nonstatic shape and orientation would be expected if the material is continuously being pulverized as it orbits the star, and/or if the newly formed small-dust particle concentrations get ejected quickly due to radiation pressure as discussed above, this quality makes matching the *Elsie* family and the *Kepler* Q16 complex a challenging task. To that end, Sacco et al. (2017) point out that the *Elsie* family dips (Figure 2) occur in an interval perhaps reminiscent of the 48.4 day putative period discussed by Boyajian et al. (2016) for the *Kepler* dip times, leading to a prediction of a 1574 day period (or a semimajor axis of 2.6 au), roughly double the period proposed by Boyajian et al. (2016). Observations in 2019 June (750 days from 2017 May) will be critical to determine whether the *Kepler* D800 event (Boyajian et al. 2016) repeats.

5. Conclusions

Given the *Kepler* data alone, it proved difficult to study this star because ground-based follow-up observations were not taken contemporaneously with the dipping events. In this paper, we show that we are able to successfully trigger a worldwide request for observations using a variety of telescopes and instruments, with different techniques, sensitivities, resolutions, and wavelengths. The main results within this paper include:

1. The photometric monitoring of KIC 8462852 is the first successful effort via crowd-funding to study an astronomical object.
2. We present the *Elsie* family of dips, a series of 1%–2.5% dips that began in 2017 May and carried on through the end of December, at the time of this paper’s writing. The *Elsie* family consists of four main dipping events, “*Elsie*,” “*Celeste*,” “*Skara Brae*,” and “*Angkor*” all of which last for several days to weeks.
3. Our observations mark the first real-time detection of a dip in brightness for KIC 8462852. Triggered spectroscopic and polarimetric observations taken during the dips reveal no large, obvious changes compared to out of dip observations.
4. Multiband photometry taken during *Elsie* show its amplitude is chromatic, with depth ratios that are consistent with occultation by optically thin dust with size scales $\ll 1 \mu\text{m}$, and perhaps with variations intrinsic to the star.

KIC 8462852 has captured the imagination of both scientists and the public. To that end, our team strives to make the steps taken to learn more about the star as transparent as possible. Additional constraints on the system will come from the triggered observations taken during the *Elsie* family of dips and beyond, which will in turn allow for more detailed modeling. Opportunities include observational projects from numerous facilities, impressively demonstrating the multidimensional approach of the community to study KIC 8462852, as mentioned within the above sections. The observed “colors” of the dips (i.e., the ratios of the dip depths in different bands)

¹³⁶ Note that $B(T)$ here represents the brightness in the B band, not the Planck function.

¹³⁷ Our analyses are also in tension with that of Foukal (2017b) on this same data set, who finds the B/i' dip depth ratio for *Elsie* to be closer to unity and more consistent with the blackbody expectation.

¹³⁸ There was no concerted monitoring effort of the star from 2013 May (when *Kepler* discontinued observations) to 2015 October.

¹³⁹ Monitoring from 2016 March up until *Elsie* by LCOGT showed no events at the $>1\%$ level. Monitoring from 2015 October up until *Elsie* by the American Association of Variable Star Observers (AAVSO) showed no events at the $>2\%$ level. These observations will be presented in a forthcoming paper.

appear inconsistent with occultation by primarily optically thick material (which would be expected to produce nearly achromatic dips) and appear to be in some tension with intrinsic cooling of the star at constant radius.

We emphasize the importance that continued monitoring will bring to our understanding of the physical processes responsible for the light-curve features. In general, precise, long-term photometric monitoring to detect future dips is a level-zero requirement. These data also provide the means of informing planned triggered observations such as high-resolution spectroscopy to study the events in more detail. Furthermore, extended photometric monitoring will enable us to characterize the star's long-term variability (Montet & Simon 2016; Schaefer 2016; Meng et al. 2017; Simon et al. 2017), which is thought to be linked to the dips in some way. All-in-all, the apparent low duty cycle of the dips, unclear predictions on when they will recur, and fairly unconstrained multiyear timescales of the long-term variability will require a committed, intensive monitoring program spanning the next decade and beyond.

The LCOGT observations used in this project were made possible by the collective effort of 1762 supporters as part of the Kickstarter campaign “The Most Mysterious Star in the Galaxy.”¹⁴⁰ The authors gratefully acknowledge and humbly extend a special thanks for substantial support from Las Cumbres Observatory, Glenn Klakring, Fred Boyajian and Bobbie Staley, Alex Mazingue, The Bible Family, Claudio Bottaccini, Joachim De Lombaert, Amity and Brigid Williams, Kevin Fischer, William Hopkins, Milton Bosch, Zipeng Wang, T.J., D.R., and C.C. The authors thank Peter Foukal for helpful conversations. A.T. wishes to acknowledge her mother, Celeste, for all her love and efforts to help her become an astronomer. A.T. also wishes to thank the Boyajian’s Star Kickstarter team for electing to name dip “*Celeste*” after her mom who passed away in 2017 June. Mom would have been pleased and would have “got it.”

H.D. acknowledges support from grant ESP2015-65712-C5-4-R of the Spanish Secretary of State for R&D&I (MINECO). This research made use of data acquired with the Gran Telescopio Canarias (GTC), installed at the Spanish Observatorio del Roque de los Muchachos of the Instituto de Astrofísica de Canarias, in the island of La Palma. J.B. acknowledges the support from the VEGA 2/0031/18 and APVV 15-0458 grants. The Center for Exoplanets and Habitable Worlds is supported by the Pennsylvania State University, the Eberly College of Science, and the Pennsylvania Space Grant Consortium. E.H.L.B.’s research was supported by an appointment to the NASA Postdoctoral Program with the Nexus for Exoplanet System Science, administered by Universities Space Research Association under contract with NASA. A.V.F.’s group is grateful for financial assistance from the TABASGO Foundation, the Christopher R. Redlich Fund, Gary and Cynthia Bengier (T.d.J. is a Bengier Postdoctoral fellow), and the Miller Institute for Basic Research in Science (U.C. Berkeley). This project was supported by the National Research, Development and Innovation Fund of Hungary, financed under the K_16 funding scheme (project No. NKFIH K-115709). The research leading to these results has received funding from the ARC

grant for Concerted Research Actions, financed by the Wallonia-Brussels Federation. M. Gillon is Research Associate at the Belgian Fonds de la Recherche Scientifique (F.R.S.-FNRS). B.D.S. acknowledges support from the National Aeronautics and Space Administration (NASA) through Einstein Postdoctoral Fellowship Award Number PF5-160143 issued by the Chandra X-ray Observatory Center, which is operated by the Smithsonian Astrophysical Observatory for and on behalf of NASA under contract NAS8-03060. E.H. and I.R. acknowledge support by the Spanish Ministry of Economy and Competitiveness (MINECO) and the Fondo Europeo de Desarrollo Regional (FEDER) through grant ESP2016-80435-C2-1-R, as well as the support of the Generalitat de Catalunya/CERCA programme. A.A.R., H.S.N., and M.J.M.G. acknowledge financial support by the Spanish Ministry of Economy and Competitiveness through projects AYA2014-60476-P and AYA2014-60833-P. F.J.P.R. is supported by Marie Curie CO-FUND fellowship, co-founded by the University of Liège and the European Union. F.P.N. is supported by grants 950/15 from the Israeli Science Foundation (ISF) and 3555/14-1 from the Deutsche Forschungsgemeinschaft (DFG).

A major upgrade of the Kast spectrograph on the Shane 3 m telescope at Lick Observatory was made possible through generous gifts from William and Marina Kast as well as the Heising-Simons Foundation. Research at Lick Observatory is partially supported by a generous gift from Google. Some of the data presented herein were obtained at the W. M. Keck Observatory, which is operated as a scientific partnership among the California Institute of Technology, the University of California, and the National Aeronautics and Space Administration (NASA); the observatory was made possible by the generous financial support of the W. M. Keck Foundation. This publication makes use of data products from the *Wide-field Infrared Survey Explorer*, which is a joint project of the University of California, Los Angeles, and the Jet Propulsion Laboratory/California Institute of Technology, funded by NASA. This publication also makes use of data products from NEOWISE, which is a project of the Jet Propulsion Laboratory/California Institute of Technology, funded by the Planetary Science Division of NASA.

Software: emcee (Foreman-Mackey et al. 2013).

Appendix Observations

A.1. Photometry

Regular monitoring of KIC 8462852 started in 2016 March with the Las Cumbres Observatory (LCOGT) 0.4 m telescope network, which has identical robotic capabilities to the LCOGT 1 m and 2 m telescope networks (Brown et al. 2013). The northern hemisphere 0.4 m network currently consists of telescopes at three sites: TFN (Canary Islands, Spain), OGG (Hawaii, USA), and since 2017 November, ELP (Texas, USA). The scheduled LCOGT requests consisted of Johnson *B* and Sloan *r'* and *i'* images, taking two exposures per sequence with a cadence of ~ 30 minutes. On JD 2,457,892 (UT 2017 May 18; UT dates are used throughout this paper), a drop in brightness was claimed as significant at more than one site. We then increased the priority and cadence of the LCOGT *Br'i'* sequence, and submitted additional *Br'i'* sequence requests for coverage on the LCOGT 1 m telescopes in Texas, USA (ELP) and California, USA (SQA) and on the 2 m telescope in

¹⁴⁰ <https://www.kickstarter.com/projects/608159144/the-most-mysterious-star-in-the-galaxy>

Hawaii, USA (OGG2). Data are automatically processed by LCOGT servers using BANZAI¹⁴¹ and transferred to local machines where we perform differential photometry for each telescope and filter image stacks using AstroimageJ (Collins et al. 2017).

Two hundred and thirty-one nightly observations of KIC 8462852 were acquired from 2016 April 15 to June 21 and again from 2016 November 12 to 2017 July 1 with the Tennessee State University Celestron 14 inch (C14) automated imaging telescope (AIT) at Fairborn Observatory. See Sing et al. (2015) for a brief description of the C14 operation and data analysis. We saw no evidence for variability in the first observing interval to a limit of a few millimagnitudes. KIC 8462852 likewise appeared to be constant in the second interval until 2017 May 18, when the C14 revealed the star had dipped in brightness around a percent. With the Fairborn and LCOGT data both showing signs of the start of a dip in brightness, an alert for triggered observations was executed.

Observations of KIC 8462852 were also made with Calvin College’s remotely operated telescope in Rehoboth, NM (Molnar et al. 2017). Images in Sloan $g'r'i'z'$ filters were taken on 10 nights, on April 26 and then for a string of 9 nights beginning May 20. We used MaxIm¹⁴² to perform differential photometry.

KIC 8462852 was observed with the Joan Oró robotic 0.8 m telescope (TJO) at the Montsec Astronomical Observatory (Catalonia). The star was regularly monitored from 2017 March 14 and the priority and cadence of the observations was increased once the drop in brightness was detected. Sequences of five images in the Johnson R filter were then obtained one to three times per night and automatically processed with the TJO reduction pipeline (Colome & Ribas 2006). Differential photometry was performed using AstroimageJ.

The 0.6 m robotic telescope TRAPPIST-North¹⁴³ (Gillon et al. 2011; Jehin et al. 2011) observed KIC 8462852 starting 2017 May 20. Each night of observation consisted of exposures of 13 and 15 s gathered within an “ $I + z$ ” filter and Johnson V filter, respectively. Data reduction was done automatically and consisted of the calibration (bias, dark, and flat field) and alignment of the images, and then of the extraction of the fluxes of selected stars by aperture photometry with the DAOPHOT software (Stetson 1987).

Observations at Thacher Observatory, on the campus of The Thacher School in Ojai, CA, began in the spring of 2017 in the Johnson V band. A variable number of observations of KIC 8462852 were performed nightly depending on the weather and telescope demand. Relative fluxes were obtained with aperture photometry and the ratio between KIC 8462852 and the sum of the seven reference stars are averaged to produce one measurement per night using a custom pipeline.

Johnson-Bessel $BVRI$ images of KIC 8462852 were acquired with the NITES telescope (McCormac et al. 2014) on La Palma. The data were reduced in Python with CCDPROC (Craig et al. 2015) using a master bias, dark, and flat. A total of 5, 5, 4, and 2 nonvariable comparison stars were used for each of the B , V , R , and I filters, and aperture photometry was extracted using SEP (Bertin & Arnouts 1996; Barbary 2016).

We obtained 60 s exposure photometry using the SBIG STX-16803 CCD mounted on the 1 m telescope of the Wise Observatory in Israel, on a total of 15 nights between 2017

May 19 and June 21. We alternated between the B , V , r' , i' , and z' filters with 3×3 binning. The images were bias, dark, and flat-field corrected using IRAF.¹⁴⁴ Aperture photometry was performed using AstroimageJ.

Spectrophotometric observations were obtained with the OSIRIS long-slit spectrograph on the 10.5 m Gran Telescopio Canarias (GTC). Between 2017 May 17 and September 9, 13 pointings were performed, all with a resolution of $R = 1000$. Each pointing consisted of a time series of about 30 minutes in duration, from individual shots with 20 s exposure time. A nearby star of similar brightness (KIC 8462763, $V = 11.86$ mag) was included in the same slit and used as reference in the photometric analysis. The target’s spectra were divided into five wavelength ranges, and the fluxes at each of these wavelengths are averages of the 30 minutes time series. A detailed description and analysis of the GTC data are presented in Deeg et al. (2018).

A.2. Spectroscopy

A.2.1. Low-resolution

Over the six-month period beginning on 2017 May 20, 14 optical spectra of KIC 8462852 were obtained with the Kast Double Spectrograph mounted on the 3 m Shane telescope (Miller & Stone 2013) at the Lick Observatory. Additional optical spectra were acquired using the 10 m Keck telescopes on 2017 May 29 with the DEep Imaging Multi-Object Spectrograph (DEIMOS; Faber et al. 2003) and again on 2017 June 25 with the LRIS (Oke et al. 1995; Rockosi et al. 2010). All spectra were taken at or near the parallactic angle (Filippenko 1982) to minimize slit losses caused by atmospheric dispersion. Data were reduced following standard techniques for CCD processing and spectrum extraction (Silverman et al. 2012) utilizing IRAF routines and custom Python and IDL codes.¹⁴⁵ Low-order polynomial fits to arc-lamp spectra were used to calibrate the wavelength scale, and small adjustments derived from night-sky lines in the target frames were applied. Observations of appropriate spectrophotometric standard stars were used to flux calibrate the spectra.

A.2.2. High-resolution

We analyzed high-resolution optical spectra taken prior to (2015 October 31, November 27–29, and 2016 August 21; five total) and during (2017 May 20–22; three total) the *Elsie* event with the High Resolution Echelle Spectrometer (HIRES; Vogt et al. 1994) on the 10 m Keck I telescope on Maunakea, Hawaii. All spectra were taken with the C2 decker and without the iodine cell (slit $14''0$ length and $0''861$ width), giving a typical resolution $R \approx 48,000$ with signal-to-noise ratios $S/N \approx 100$ –150 per pixel. The spectra cover the following wavelength ranges: pre-dip 3643–7990 Å, in-dip (2017 May 20–21) 3833–6656 Å, and in-dip (2017 May 22) 3101–5987 Å.

ORCID iDs

Tabetha. S. Boyajian  <https://orcid.org/0000-0001-9879-9313>
 Geoffrey C. Clayton  <https://orcid.org/0000-0002-0141-7436>
 James R. A. Davenport  <https://orcid.org/0000-0002-0637-835X>















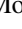


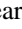





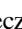
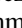




¹⁴¹ <https://github.com/LCOGT/banzai>

¹⁴² <http://diffractionlimited.com/product/maxim-dl>

¹⁴³ <http://www.trappist.uliege.be>

¹⁴⁴ IRAF is distributed by the National Optical Astronomy Observatory, which is operated by AURA, Inc., under a cooperative agreement with the NSF.

¹⁴⁵ <https://github.com/ishivvers/TheKastShiv>

J. Farihi  <https://orcid.org/0000-0003-1748-602X>
 Na'ama Hallakoun  <https://orcid.org/0000-0002-0430-7793>
 Ottó Hanyecz  <https://orcid.org/0000-0002-9415-5219>
 Grant M. Kennedy  <https://orcid.org/0000-0001-6831-7547>
 H. Korhonen  <https://orcid.org/0000-0003-0529-1161>
 Levente Kriskovics  <https://orcid.org/0000-0002-1792-546X>
 Gavin P. Lamb  <https://orcid.org/0000-0001-5169-4143>
 Marie Wingyee Lau  <https://orcid.org/0000-0001-9755-9406>
 Chris Lintott  <https://orcid.org/0000-0001-5578-359>
 Carey Lisse  <https://orcid.org/0000-0002-9548-1526>
 Massimo Marengo  <https://orcid.org/0000-0001-9910-9230>
 Joseph R. Masiero  <https://orcid.org/0000-0003-2638-720X>
 Huan Y. A. Meng  <https://orcid.org/0000-0003-0006-7937>
 Lawrence A. Molnar  <https://orcid.org/0000-0002-5472-4181>
 Brett M. Morris  <https://orcid.org/0000-0003-2528-3409>
 John M. O'Meara  <https://orcid.org/0000-0002-7893-1054>
 András Pál  <https://orcid.org/0000-0001-5449-2467>
 F. Pozo Nuñez  <https://orcid.org/0000-0002-6716-4179>
 Seth Redfield  <https://orcid.org/0000-0003-3786-3486>
 Joonas L. O. Saario  <https://orcid.org/0000-0003-0780-9825>
 Emily J. Safron  <https://orcid.org/0000-0002-6872-2582>
 Krisztián Sárneczky  <https://orcid.org/0000-0003-0926-3950>
 Brooke D. Simmons  <https://orcid.org/0000-0001-5882-3323>
 Geoff Stone  <https://orcid.org/0000-0001-5888-9162>
 Róbert Szabó  <https://orcid.org/0000-0002-3258-1909>
 Róbert Szakáts  <https://orcid.org/0000-0002-1698-605X>
 Krisztián Vida  <https://orcid.org/0000-0002-6471-8607>
 József Vinkó  <https://orcid.org/0000-0001-8764-7832>
 Jason T. Wright  <https://orcid.org/0000-0001-6160-5888>

References

- Ballesteros, F. J., Amalte-Mur, P., Fernandez-Soto, A., & Martinez, V. J. 2018, *MNRAS*, **473**, L21
- Barbary, K. 2016, SEP: Source Extractor as a library, <http://joss.theoj.org/papers/10.21105/joss.00058>
- Bertin, E., & Arnouts, S. 1996, *A&AS*, **117**, 393
- Bessell, M. S. 1990, *PASP*, **102**, 1181
- Bodman, E. H. L., & Quillen, A. 2016, *ApJL*, **819**, L34
- Borucki, W. J., Koch, D., Basri, G., et al. 2010, *Sci*, **327**, 977
- Boyajian, T. S., LaCourse, D. M., Rappaport, S. A., et al. 2016, *MNRAS*, **457**, 3988
- Brown, T. M., Baliber, N., Bianco, F. B., et al. 2013, *PASP*, **125**, 1031
- Budaj, J., Kocifaj, M., Salmeron, R., & Hubeny, I. 2015, *MNRAS*, **454**, 2
- Castelli, F., & Kurucz, R. L. 2004, arXiv:astro-ph/0405087
- Claret, A., & Bloemen, S. 2011, *A&A*, **529**, A75
- Collins, K. A., Kielkopf, J. F., Stassun, K. G., & Hessman, F. V. 2017, *AJ*, **153**, 77
- Colome, J., & Ribas, I. 2006, *IAUSS*, **6**, 11
- Craig, M. W., Crawford, S. M., Deil, C., et al. 2015, ccdproc: CCD data reduction software, Astrophysics Source Code Library, ascl:1510.007
- Curtis, J. L. 2017, *AJ*, **153**, 275
- Cutri, R. M., Mainzer, A., Conrow, T., et al. 2015, Explanatory Supplement to the NEOWISE Data Release Products, Tech. Rep., <http://wise2.ipac.caltech.edu/docs/release/neowise/expsup>
- Deeg, H. J., Alonso, R., Nespral, D., & Boyajian, T. 2018, *A&A*, in press (arXiv:1801.00720)
- Deirmendjian, D. 1964, *ApOpt*, **3**, 187
- Dorschner, J., Begemann, B., Henning, T., Jaeger, C., & Mutschke, H. 1995, *A&A*, **300**, 503
- Faber, S. M., Phillips, A. C., Kibrick, R. I., et al. 2003, *Proc. SPIE*, **4841**, 1657
- Filippenko, A. V. 1982, *PASP*, **94**, 715
- Foreman-Mackey, D., Hogg, D. W., Lang, D., & Goodman, J. 2013, *PASP*, **125**, 306
- Foukal, P. 2017a, *ApJL*, **842**, L3
- Foukal, P. 2017b, *RNAAS*, **1**, 52
- Gillon, M., Jehin, E., Magain, P., et al. 2011, *EPJWC*, **11**, 06002
- Harp, G. R., Richards, J., Shostak, S., et al. 2016, *ApJ*, **825**, 155
- Heiles, C. 2000, *AJ*, **119**, 923
- Hipke, M., Angerhausen, D., Lund, M. B., Pepper, J., & Stassun, K. G. 2016, *ApJ*, **825**, 73
- Jäger, C., Dorschner, J., Mutschke, H., Posch, T., & Henning, T. 2003, *A&A*, **408**, 193
- Jager, C., Mutschke, H., & Henning, T. 1998, *A&A*, **332**, 291
- Jehin, E., Gillon, M., Queloz, D., et al. 2011, *Msngr*, **145**, 2
- Johnson, P. B., & Christy, R. W. 1974, *PhRvB*, **9**, 5056
- Katz, J. I. 2017, *MNRAS*, **471**, 3680
- Kiefer, F., Lecavelier des Etangs, A., Vidal-Madjar, A., et al. 2017, *A&A*, **608**, A132
- Koike, C., Kaito, C., Yamamoto, T., et al. 1995, *Icar*, **114**, 203
- Lisse, C. M., Sitko, M. L., & Marengo, M. 2015, *ApJL*, **815**, L27
- Makarov, V. V., & Goldin, A. 2016, *ApJ*, **833**, 78
- Mandel, K., & Agol, E. 2002, *ApJL*, **580**, L171
- Marengo, M., Hulsebus, A., & Willis, S. 2015, *ApJL*, **814**, L15
- Mauerhan, J., Williams, G. G., Smith, N., et al. 2014, *MNRAS*, **442**, 1166
- McCormac, J., Skillen, I., Pollacco, D., et al. 2014, *MNRAS*, **438**, 3383
- Meng, H. Y. A., Rieke, G., Dubois, F., et al. 2017, *ApJ*, **847**, 131
- Metzger, B. D., Shen, K. J., & Stone, N. 2017, *MNRAS*, **468**, 4399
- Miller, J. S., & Stone, R. P. S. 2013, Lick Obs. Tech. Rep. 66
- Molnar, L. A., Van Noord, D. M., Kinemuchi, K., et al. 2017, *ApJ*, **840**, 1
- Montet, B. T., & Simon, J. D. 2016, *ApJL*, **830**, L39
- Neslušan, L., & Budaj, J. 2017, *A&A*, **600**, A86
- Oke, J. B., Cohen, J. G., Carr, M., et al. 1995, *PASP*, **107**, 375
- Pecaut, M. J., & Mamajek, E. E. 2013, *ApJS*, **208**, 9
- Pecaut, M. J., Mamajek, E. E., & Bubar, E. J. 2012, *ApJ*, **746**, 154
- Rockosi, C., Stover, R., Kibrick, R., et al. 2010, *Proc. SPIE*, **7735**, 77350R
- Sacco, G., Ngo, L., & Modolo, J. 2017, arXiv:1710.01081
- Savage, B. D., & Mathis, J. S. 1979, *ARA&A*, **17**, 73
- Schaefer, B. E. 2016, *ApJL*, **822**, L34
- Schmidt, G. D., Elston, R., & Lupie, O. L. 1992, *AJ*, **104**, 1563
- Serkowski, K., Mathewson, D. S., & Ford, V. L. 1975, *ApJ*, **196**, 261
- Sheikh, M. A., Weaver, R. L., & Dahmen, K. A. 2016, *PhRvL*, **117**, 261101
- Silverman, J. M., Foley, R. J., Filippenko, A. V., et al. 2012, *MNRAS*, **425**, 1789
- Simon, J. D., Shappee, B. J., Pojmanski, G., et al. 2017, arXiv:1708.07822
- Sing, D. K., Wakeford, H. R., Showman, A. P., et al. 2015, *MNRAS*, **446**, 2428
- Stowikowska, A., Krzeszowski, K., Żejmo, M., Reig, P., & Steele, I. 2016, *MNRAS*, **458**, 759
- Steele, I. A., Copperwheat, C. M., Jermak, H. E., Kennedy, G. M., & Lamb, G. P. 2018, *MNRAS*, **473**, L26
- Stetson, P. B. 1987, *PASP*, **99**, 191
- Thompson, M. A., Scicluna, P., Kemper, F., et al. 2016, *MNRAS*, **458**, L39
- Vogt, S. S., Allen, S. L., Bigelow, B. C., et al. 1994, *Proc. SPIE*, **2198**, 362
- Wallace, L., Hinkle, K. H., Livingston, W. C., & Davis, S. P. 2011, *ApJS*, **195**, 6
- Warren, S. G., & Brandt, R. E. 2008, *JGRD*, **113**, D14220
- Wright, J. T., & Eastman, J. D. 2014, *PASP*, **126**, 838
- Wright, J. T., & Sigurdsson, S. 2016, *ApJL*, **829**, L3
- Wyatt, M. C., van Lieshout, R., Kennedy, G. M., & Boyajian, T. S. 2018, *MNRAS*, **473**, 5286